



## Article

# A Study on the Dynamic Collision Behaviors of a Hydrous Ethanol Droplet on a Heated Surface

Ze Zhou <sup>1,2</sup>, Fuwu Yan <sup>1,\*</sup>, Gengxin Zhang <sup>2</sup> , Dawei Wu <sup>2,\*</sup>  and Hongming Xu <sup>2</sup>

<sup>1</sup> Hubei Key Laboratory of Advanced Technology for Automotive Components, School of Automotive Engineering, Wuhan University of Technology, Wuhan 430070, China; ze.zhou@whut.edu.cn

<sup>2</sup> Department of Mechanical Engineering, School of Engineering, University of Birmingham, Birmingham B15 2TT, UK; g.zhang.6@bham.ac.uk (G.Z.); h.m.xu@bham.ac.uk (H.X.)

\* Correspondence: yanfuwu@vip.sina.com (F.Y.); d.wu.1@bham.ac.uk (D.W.)

**Abstract:** This study uses high-speed imaging to investigate the dynamic collision behavior of a single hydrous ethanol droplet in different water/ethanol ratios on a heated horizontal glass surface. The initial droplet diameter varied from 3.3 to 4.1 mm, and the impact velocity was 0.57 m/s. The study covers a range of surface temperatures (373 K to 553 K) and ethanol mass fractions (0% to 100%) to reveal four regimes of droplet-impinging behaviors, including quiescent surface evaporation, puffing or partial boiling, explosive nuclear boiling, and the Leidenfrost effect. The addition of volatile ethanol to less volatile water shifts the droplet collision behavior toward explosive boiling and the Leidenfrost phenomenon. As the ethanol mass fraction increased from 0% to 100%, the superheat limit temperature decreased by approximately 80 K, while the Leidenfrost temperature decreased by at least 100 K. The dimensionless droplet diameter in the regime of droplet spreading with quiescent surface evaporation is influenced by surface temperature, surface tension, and viscosity. Meanwhile, the dimensionless diameter and height of a droplet in the regime of the Leidenfrost phenomenon are mainly influenced by its surface tension. The study concludes that a single parameter, such as the superheat level, Weber number, or Reynolds number, is difficult to describe droplet collision behavior, and multiple factors would be required to best describe droplet collision behavior and establish empirical correlations. However, it is feasible to predict partial collision behaviors by using one of the single parameters under certain conditions.



**Citation:** Zhou, Z.; Yan, F.; Zhang, G.; Wu, D.; Xu, H. A Study on the Dynamic Collision Behaviors of a Hydrous Ethanol Droplet on a Heated Surface. *Processes* **2023**, *11*, 1804. <https://doi.org/10.3390/pr11061804>

Academic Editor: Albert Ratner

Received: 27 April 2023

Revised: 6 June 2023

Accepted: 8 June 2023

Published: 14 June 2023



**Copyright:** © 2023 by the authors. Licensee MDPI, Basel, Switzerland. This article is an open access article distributed under the terms and conditions of the Creative Commons Attribution (CC BY) license (<https://creativecommons.org/licenses/by/4.0/>).

**Keywords:** droplet collision; high-speed imaging; heated surface; explosive boiling; Leidenfrost effect

## 1. Introduction

The impact of spray on walls has been widely observed in various applications, such as spray cooling for heat-generating components [1,2] and fuel sprays in internal combustion engines [3–5]. The process of droplets impacting walls is highly complicated, involving the theories of fluid mechanics and surface material, as well as heat and mass transfer processes on temperature-elevated walls. Several studies have been conducted on spray-wall impingement. Liu et al. [6] conducted an experimental study on the heat transfer performance of spray-wall collision during the ethanol spray cooling process. Luo et al. [7,8] focused on the spray-wall impact characteristics of engine fuels and conducted a series of related studies. However, the spray collision process involves the impact of multiple droplets on a solid surface, making it difficult to directly observe the behavior of each droplet during the instantaneous wall collision process.

To investigate the underlying mechanism of spray-wall collision, an experimental study of a single-droplet collision on a wall is required, which allows the researchers to conduct a visual detection of individual droplet attachment or splash behavior using high-speed photography and enables a more detailed analysis of individual droplet behaviors. Such an approach provides crucial experimental evidence for the fundamental understanding and numerical simulation of the spray-wall impact phenomenon. Mundo et al. [9]

performed a single-droplet impact experiment and proposed the concept of liquid droplet deposition and splashing. An et al. [10] observed the impact process of droplets with varying physical properties on walls with different levels of wettability at different velocities. Their analysis revealed that droplets with high viscosity exhibit a smaller maximum spreading diameter, and the impact velocity has a greater impact on the maximum spreading radius of droplets with low viscosity, while wall wettability has a minimal effect. Andrade et al. [11] conducted an experimental study on the impact patterns of three different liquid droplets with varying physical properties hitting various surfaces. Their experiments were conducted under the following conditions: the pre-impact diameters of the droplets ranged from 3.00 to 3.65 mm and the Weber number varied from 100 to 800, whereas the Reynolds number ranged from 1000 to 12,500. The results showed that both the viscosity and surface material properties had a significant impact on the dynamic characteristics of droplet impact. Furthermore, the viscosity of the droplet played a crucial role in its spreading and retracting process. Abubakar et al. [12,13] studied the effect of droplet size on impact characteristics on a flat hydrophobic surface. They reported that increasing the size of the droplet results in an enlargement of the wetting diameter on the impacted surface. They also investigated the impact of water droplets on a hydrophobic mesh surface and analyzed properties such as spreading, rebounding, droplet fluid penetration, and ejection rates. Their findings revealed that the contact time of impacting droplets over the mesh surface decreased when the droplet Weber number increased, which was quite different from the results observed for impacting droplets on flat hydrophobic surfaces. Josserand et al. [14] and Yarin et al. [15] studied the droplet impact dynamics on a dry solid surface. They found that droplet impact behavior is related to the distance from the impact center to the droplet's initial position. The walls investigated in all the above studies are cold walls with surface temperatures below the boiling point of the droplets. The characteristics of droplet collision on these walls are mainly influenced by factors including droplet velocity, viscosity, surface tension, and surface properties of the walls.

Compared to the impact on a cold wall, the collision on a hot surface becomes more complicated due to the phase change and boiling of the droplet. With the elevation of substrate surface temperature, the dominant mechanism of droplet phase change during the impact process transforms from initial evaporation to nucleate boiling and ultimately to film boiling [16–18]. The transformation of the phase change form greatly influences the droplet collision behaviors, so related research was mainly carried out around this. Grissom et al. [19] experimentally and theoretically studied the water spray cooling on the heated surface, and they revealed that the initiation of the Leidenfrost state sets the upper temperature limit for spray evaporative cooling on the surface. Qiao et al. [20] conducted an experimental investigation on the impact of surfactant concentration on droplets boiling on a hot stainless-steel surface. They found that an increase in surfactant concentration resulted in a decrease in the Leidenfrost temperature. This temperature corresponds to the point at which droplets levitate above the surface on a thin film of their own vapor. Chandra et al. [21] used both experiments and numerical modeling to study the cooling of a hot wall through the evaporation of liquid droplets (the surface temperature ranged from 60 °C to 110 °C), and they suggested that reducing the contact angle can reduce the droplet evaporation time and improve the spray cooling performance. Fujimoto et al. [22] used a two-directional flash photography technique to investigate the collision of single water droplets on a hot alloy surface. Their experiments were conducted under the following conditions: the pre-impact diameters of the droplets ranged from 0.53 to 0.60 mm, the impact velocities ranged from 1.7 m/s to 4.1 m/s, and the solid surface temperatures ranged from 170 °C to 500 °C. Their research revealed that vapor bubbles form at the liquid–solid interface under heterogeneous boiling conditions, where the interfacial temperature is below the superheat limit. Li et al. [23] conducted an experimental study on the impact of the Leidenfrost dynamics of water droplets on a heated post (the surface temperature ranged from 120 °C to 330 °C and the Weber numbers ranged from 10 to 120), revealing the influence of the post structure and surface inclination. Roisman and Tropea et al. [24]

conducted an experimental study on the mechanisms of the thermal atomization of a drop impacting onto a hot substrate. They found that the atomization of droplets is characterized by the wetting and dewetting of the substrate, which is caused not by the rim dynamics but induced by thermal effects. Notably, only single-component droplets are employed to be studied in the above references.

In most industrial applications, the working mediums, such as cooling sprays or liquid fuels, typically consist of multiple components [6,25–27]. The proportion of components in a multi-component droplet has a great effect on its physical properties. These physical properties significantly influence droplet collision behaviors. Due to the evaporation of multi-component droplets when colliding on the heated surface, the mutual influence of multi-component phase changes, and the concurrent variation in droplet concentration further complicates the dynamic droplet collision. Liu et al. [6] and Zhang et al. [25] experimentally explored the heat transfer performance of an alcohol–water solution (alcohol mass fraction ranged from 0% to 10%) spray upon impingement with a wall. However, both studies mainly focused on the macroscopic heat transfer characteristic of the spray collision, without any further observation of a single-droplet collision behavior. Blanken et al. [28] and Piskunov et al. [29] studied the explosion process of multi-component droplets, which are immiscible with each other, impacting a heated wall. However, in their work, only the low boiling point component evaporates firstly within the droplets; therefore, each component evaporates independently within the droplets, and there is no interaction between them. Additionally, the shift between different dominant mechanisms of the phase change process exerts a significant influence on droplet collision behaviors. There is a clear literature gap of crucial experimental evidence to deepen fundamental understanding of the dominant mechanism of the droplet phase change along with the component proportion change during the impact process.

In this paper, we investigated the behaviors of droplets colliding with a heated wall by using a typical multi-component solution of ethanol–water as the testing medium. To fully observe all the droplet collision forms, this study implemented several innovations in experimental design. Firstly, this study employed an optically flat glass slide as the temperature-elevated surface with a high level of cleanliness, smoothness, and hydrophilicity, which can provide a high superheat limit temperature and Leidenfrost temperature. Secondly, this study employed a wide range of solution concentrations (ethanol mass fraction from 0% to 100%). The above two points, combined with a wide range of substrate temperatures (a surface temperature from 373 K to 553 K), allow for a comprehensive investigation of the effects of the concentration on droplet behavior. A high-speed imaging system was performed to analyze the droplet collision behaviors. Based on the experimental findings, we conducted a comprehensive analysis of each collision behavior and its underlying mechanisms. Additionally, based on the comprehensive results obtained from the experiment, we analyzed the generality of several parameters in describing droplet collision behaviors.

## 2. Methodology

### 2.1. Experiment Setup

The experimental setup is shown schematically in Figure 1. All experiments were conducted at atmospheric pressure. All the droplet impact tests were carried out on a piece of 1 mm thick, finely washed, and cleaned low-iron optical glass slide (VWR-BS7011, USA). A new piece of dry glass slide was used before each experiment to keep a clean surface without any surface alteration by the testing hydrous ethanol solution. The arithmetic mean of the glass slide surface roughness was measured to be within 1.2 nm by an atomic force microscope (Bruker-AXS, Karlsruhe, Germany). The glass slide was placed horizontally and tightly on a metal base with an embedded electric heater. To accurately measure the surface temperature, a thermocouple was closely attached to the glass surface. The thermocouple was installed near the long side of the glass slide to avoid the influence of droplet cooling on temperature measurement. A temperature controller (RS-ESM-7720,

UK) with a PID control system was implemented to maintain a precise and constant surface temperature throughout the experiment. The deviation from the preset temperature during the experiments was within  $\pm 5^\circ\text{C}$ .

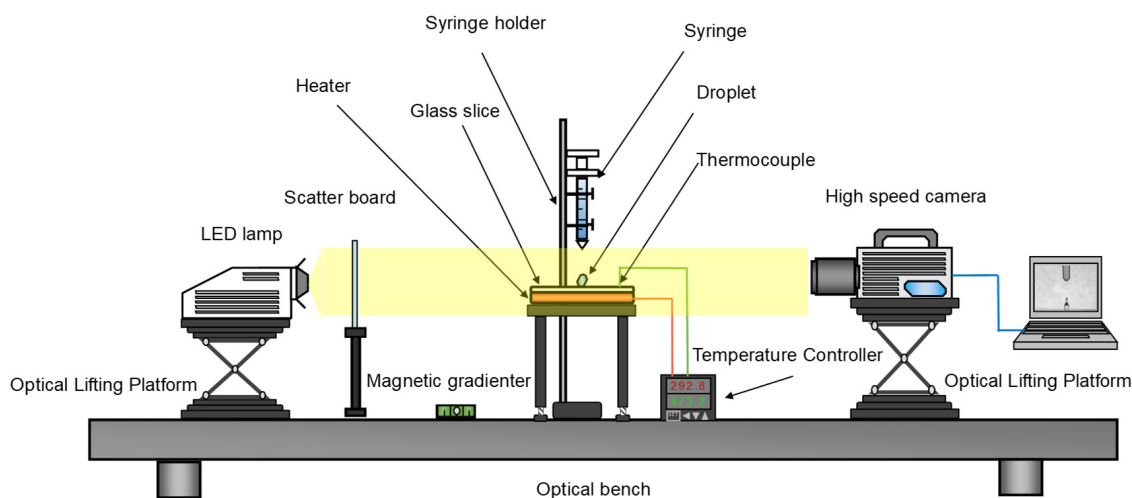


**Figure 1.** Schematic of the experiment setup.

A droplet was generated by exerting pressure on a 1 mL syringe (TERUMO-SS01T1, Japan) with a 4.0 mm outer diameter and a 1.1 mm inner diameter tip. The flow rate was carefully adjusted to allow droplet formation at the tip, and its detachment was facilitated by the force of gravity. The syringe's tip was placed by a syringe holder at a height of 16.7 mm from the glass surface. Based on the estimation of the Weber number and the results of the pre-test, it was ascertained that the droplet has a small Weber number (Weber number  $< 40$ ), and its kinetic energy upon impact with the surface at this height was insufficient to cause fragmentation or rupture.

Due to the rapid and transient nature of droplet deformation and boiling phenomenon, high-speed photography was employed in this study. The droplet impact process was captured using a high-speed camera (Phantom-V710, Japan) at a frame rate of 6000 fps with an image resolution of  $512 \times 384$  pixels. A 150 W LED light source was utilized with a backlit imaging technique. All experimental equipment was mounted on an optical bench and leveled horizontally using a gradienter.

## 2.2. Droplet Properties and Test Conditions

In this study, hydrous ethanol solutions were used as the test fluid, as such solutions are typical examples of non-ideal binary solutions. The experiment tested three different ethanol concentrations, specifically  $\omega_e = 30\%$ ,  $\omega_e = 50\%$ , and  $\omega_e = 70\%$ , and all of them were below the azeotropic concentration. Within this concentration range, ethanol behaves as a volatile component in the solution. Additionally, pure ethanol and pure water were tested for comparison. The solutions were mixed by liquid mass, where, for example,  $\omega_e = 70\%$  indicates that the solution contains 70% ethanol and 30% water by weight. Figure 2 provides the physical properties of the tested fluids, which were calculated by using the NRTL-HOC equation in Aspen Plus, and the calculated results are highly accurate [30,31].

The initial droplet diameter was calculated by measuring the volume difference of the liquid level scale on the needle tube before and after the droplet falls. For each concentration, five recordings were conducted, and the average diameter was calculated from the corresponding readings. The initial droplet diameter varied from 3.3 to 4.1 mm in this study. The average measurement errors of the initial droplet diameter at each concentration were less than 0.5%, which indicates that the experimental error is small and repeatability is high. As the tip of the syringe was 16.7 mm above the glass surface,

according to the free fall equation, the velocity of the droplet impacting the surface was  $v = 0.57$  m/s.

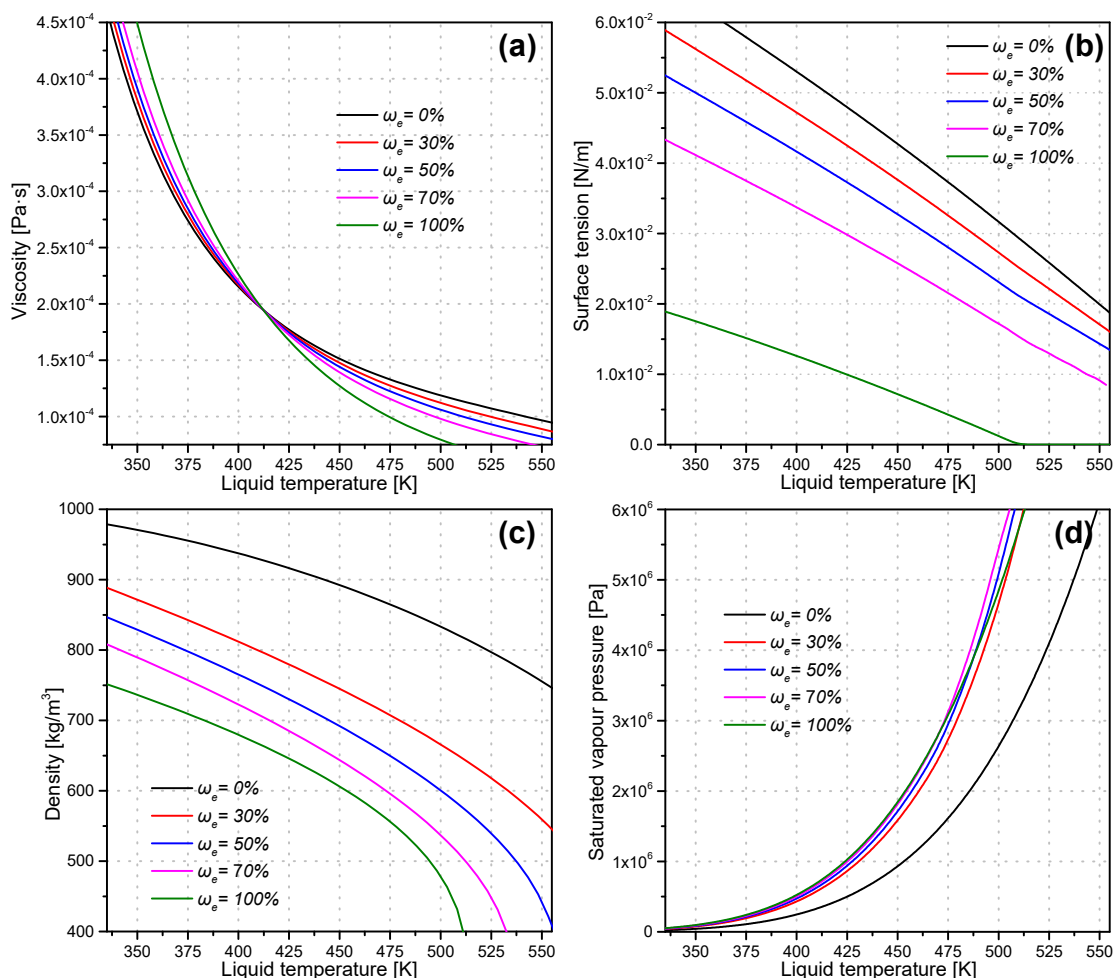


**Figure 2.** Physical properties of the tested fluids. (a) Viscosity, (b) surface tension, (c) density, (d) saturated vapor pressure.

All experiments were conducted at atmospheric pressure. The glass surface temperature ( $T_{surface}$ ) ranged from 373 K to 553 K, and the ethanol mass fraction ( $\omega_e$ ) varied from 0% to 100%. A summary of the experimental conditions is presented in Table 1.

**Table 1.** Experimental conditions.

Item	Specifications
Test fluid [-]	Ethanol/Water
Ethanol mass fraction [%]	0/30/50/70/100
Surface temperature [K]	373/393/413/433/453/473/493/513/533/553
Surface roughness [nm]	1.2
Frame rate [fps]	6000
Exposure time [ $\mu$ s]	120
Resolution [pixel]	512 $\times$ 384

### 2.3. The Parameters Related to Droplet Collision Behavior

As a droplet collides with a hot solid surface, its collision behavior is mainly affected by two factors [16,22,32]. Firstly, supercooled liquid droplets are heated through heat transfer from the hot surface, and the difference in the solid surface temperature will lead to varying dominant mechanisms of droplet phase change, which further leads to different

collision behaviors. Secondly, the deformation and fragmentation behavior of the droplet during collision is also influenced by the combined effects of its inertial force, surface tension, and viscous force.

In this paper, the superheat level of the droplet at the substrate surface temperature was utilized to characterize the effect of surface temperature, which can be expressed by a non-dimensional parameter  $R_p$ .  $R_p$  can be calculated as:

$$R_p = P_{sat} / P_{amb} \quad (1)$$

where  $P_{sat}$  is the saturation pressure of the droplet at the surface temperature and  $P_{amb}$  is the ambient pressure. The values of  $R_p$  at all surface temperature conditions are provided in Table 2 for reference, and it should be noted that the actual temperature of the droplet during impact might be lower than the surface temperature due to thermal inertia.

**Table 2.**  $R_p$  over the experimental conditions.

$R_p$	Ethanol Mass Fraction [%]					
	0	30	50	70	100	
	373	1.0	1.8	2.0	2.1	2.2
	393	1.9	3.4	3.8	4.0	4.2
	413	3.5	6.2	6.8	7.2	7.4
	433	6.0	10.4	11.3	12.0	12.3
Surface temperature	453	9.8	16.7	18.1	19.1	19.4
( $T_{surface}$ )	473	15.3	25.8	27.8	29.2	29.3
[K]	493	22.8	39.8	43.3	46.3	-
	513	32.9	60.1	64.5	67.0	-
	533	46.2	82.2	87.1	91.0	-
	553	63.3	108.1	114.9	120.5	-

In addition to superheat level, other two widely used non-dimensional parameters [15,33–35], the Weber number and the Reynolds number, were also utilized in this paper to characterize the level of combined effects of droplet inertia, surface tension, and viscosity forces. The Weber number and the Reynolds number can be calculated as:

$$\text{Weber number} = \rho v^2 d_0 / \sigma \quad (2)$$

$$\text{Reynolds number} = \rho v d_0 / \mu \quad (3)$$

where  $v$  is the droplet velocity right before impacting;  $d_0$  is the initial droplet diameter; and  $\rho$ ,  $\sigma$ , and  $\mu$  are the fluid density, surface tension, and viscosity for a fluid–air interface at room temperature (298 K), respectively. The calculated Weber and Reynolds numbers are presented in Table 3 as a reference, and it also should be noted that these are estimated values because the actual temperature of the droplet right before impacting should be higher than room temperature due to heat transfer.

**Table 3.** The Weber and Reynolds numbers.

	Ethanol Mass Fraction [%]				
	0	30	50	70	100
Weber number	14.67	15.21	16.29	18.80	38.74
Reynolds number	2547.42	1868.62	1747.87	1621.11	1394.05

#### 2.4. Image Processing

For image processing, the time when the liquid droplet makes initial contact with the glass surface was defined as time zero. The extraction of droplet spatial-resolved sizes



from original images was accomplished through the use of an in-house MATLAB code, and the procedures of image processing are illustrated in Figures 3 and 4. Figure 3a displays a typical droplet impact image, while Figure 3b illustrates the image after processing. These steps included background subtraction and contrast enhancement, followed by the binarization of the intensified image through the application of a threshold value determined by Otsu's method [36]. The resulting image enabled droplet edge identification, and we defined the droplet spreading diameter ( $d$ ) as the maximum width from the left to the right edge, which is shown in Figure 3b. Finally, the spreading diameter ( $d$ ) and height ( $h$ ) of the droplets were calculated by counting the number of their pixels and multiplying this value by the calibrated scale. The calibration of the pixels to the actual size scale is illustrated in Figure 4, the scale was established by correlating the known outer diameters of the syringe tips ( $d_{syr\_real} = 4.0$  mm) with their respective pixels ( $d_{syr\_img}$ ), as shown in Equation (4).

$$Scale = d_{syr\_real} / d_{syr\_img} \quad (4)$$

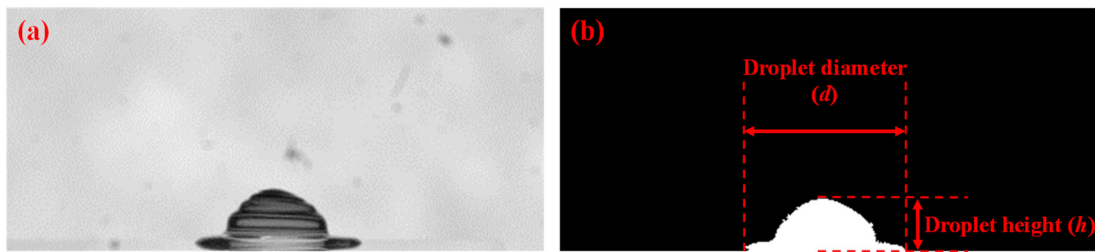


**Figure 3.** Display of image processing. (a) the original droplet image, (b) the edge of the droplet.

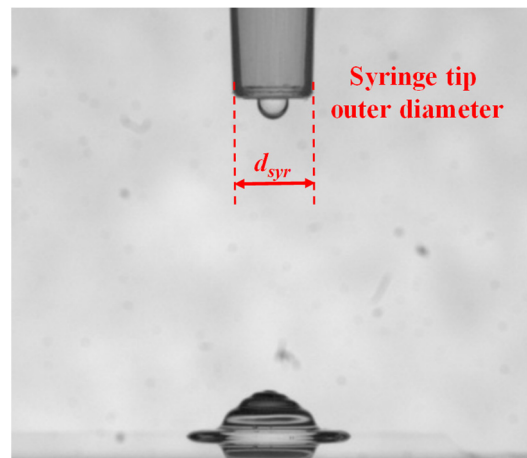


**Figure 4.** The calibration of pixels to the actual size scale.

To eliminate the influence of the initial diameter difference, in this paper, the droplet collision behaviors will be discussed by the dimensionless spreading diameter, height, and time. The dimensionless spreading diameter ( $\delta$ ) and height ( $\eta$ ) are normalized by the before-impact diameter of a droplet, as expressed in Equations (5) and (6). The dimensionless time ( $\tau$ ), as expressed in Equation (7), is normalized by the characteristic time for the impact inertia of droplets.

$$\Delta = d / d_0 \quad (5)$$

$$\eta = h / d_0 \quad (6)$$

$$\tau = tv / d_0 \quad (7)$$

where  $d_0$  is the initial droplet diameter,  $v$  is the droplet velocity right before impacting, and  $t$  is the time elapsed after the droplet contacts the surface.

### 3. Results and Discussion

#### 3.1. Overview of Droplet-Impinging Behaviors

Figure 5 presents a comprehensive overview of the droplet behaviors over the experimental conditions. As the primary focus of this study is the dynamic behavior of droplets during the impinging process, the droplet images utilized in this section were captured 10 ms after initiating impact when all test droplets had entered the stable spreading development stage.

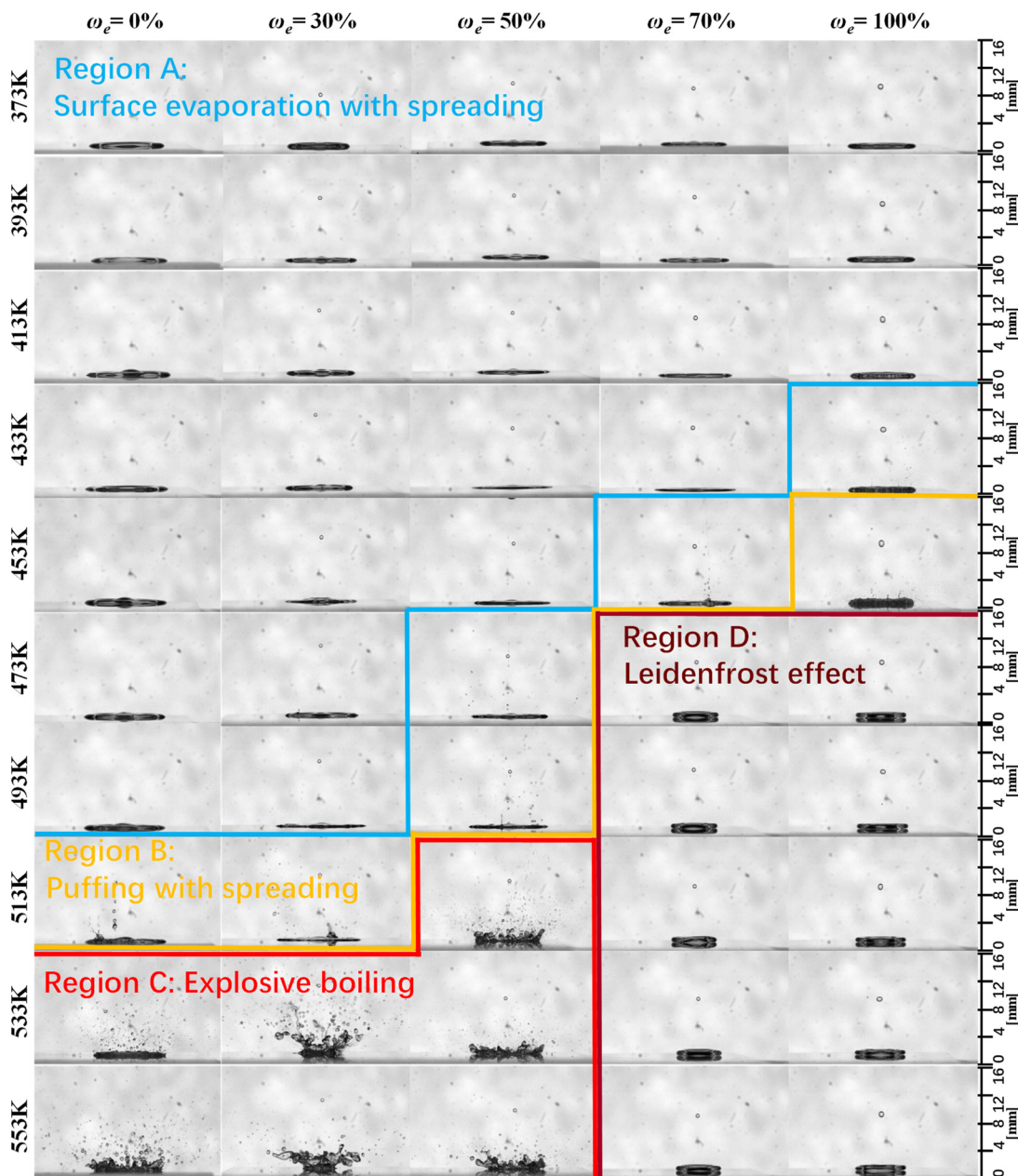


Figure 5. Overview of droplet behaviors.

As shown in Figure 5, an increase in substrate surface temperature results in a transformation of droplet behavior from initial quiescent spread to boiling after the collision, culminating in the manifestation of the Leidenfrost effect. Similarly, an analogous phe-



nomenon arises with the increase in ethanol (volatile component) proportion in the solution. This shift in droplet behavior can be attributed to the alteration of the dominant mechanism of droplet phase change from surface evaporation to nuclear boiling, and eventually to film boiling as the superheat level rises, leading to different dynamic collision behaviors of droplets. Moreover, this phenomenon also indicates the fact that the superheat limit temperature and Leidenfrost temperature of the hydrous ethanol decline as the proportion of ethanol (volatile component) increases. Specifically, as the ethanol proportion increased from  $\omega_e = 0\%$  to  $\omega_e = 100\%$ , the superheat limit temperature decreased by approximately 80 K, while the Leidenfrost temperature decreased by at least 100 K.

Based on the analysis of droplet behaviors, four distinct droplet behavior regions have been identified and labeled as A, B, C, and D, as depicted in Figure 5. In region A, upon collision with the hot surface, the droplet spreads, resulting in the formation of a liquid film that evaporates simultaneously. In region B, a liquid film forms and evaporates concurrently during the droplet's collision and spreading process, while puffing or partial boiling are also observed at the same time. In region C, the droplet undergoes explosively flashing boiling upon collision with the hot surface, resulting in the formation of a coronal splashing. In region D, a stable vapor film covers the heated surface, and this vapor film separates the droplet from the hot surface, resulting in the Leidenfrost phenomenon.

The following sections will provide a comprehensive analysis and detailed discussion of the collision behavior and underlying mechanisms for the four regimes identified above.

### 3.2. Droplet-Impinging Behaviors in Region A

Figure 6 depicts the collision process of a droplet in region A. Upon impact with the hot surface, the droplet spreads outward from the point of impact. Subsequently, the droplet reaches its maximum diameter and remains in a stable state without retracting or bouncing back. This behavior can be attributed to the rapid increase in internal pressure at the point of impact, which causes the droplet to relieve the pressure by expanding outward. The good wettability of the liquid on the solid surface and the interaction of the liquid–solid interface help the droplet maintain its state without retracting. After that, the droplet's diameter gradually reduces in size due to evaporation. The droplet does not break up during the entire process. The droplet's Weber number was small for all test conditions, indicating that the droplet would not break up due to collision. Furthermore, the smooth and clean surface with a temperature far lower than the superheat limit temperature for the liquid droplets prevents any boiling-induced break-up. The upper part of the droplet shows the slightly ring-shaped ripples in the pictures captured at 3.0 ms and 4.5 ms, possibly due to the compression of the liquid during the impact.

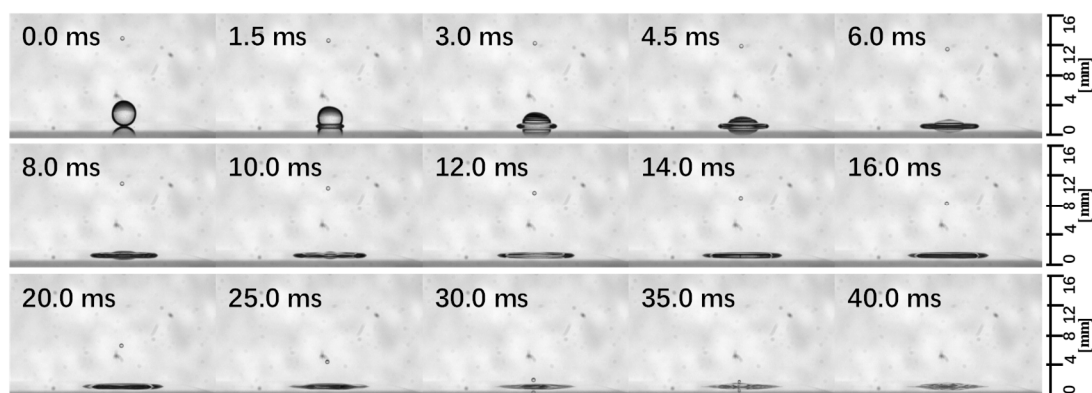


**Figure 6.** Photo sequence of the collision behavior in region A ( $\omega_e = 50\%$ ,  $T_{surface} = 393 \pm 5$  K).

Figure 7 presents the effect of substrate surface temperature on the dimensionless spreading diameter of the droplet with three different ethanol proportions. In Figure 7a,b, it can be seen that when the ethanol proportion is at  $\omega_e = 0\%$  and  $\omega_e = 50\%$ , respectively, the

droplet spreading diameter just increases as the surface temperature increases. However, in Figure 7c, it can be seen that when the ethanol proportion is at  $\omega_e = 100\%$ , the dimensionless spreading diameter of the droplet first increases and then decreases with the increase in the surface temperature. The observed phenomena can be attributed to several factors. As the surface temperature increases, heat transfer to the droplets intensifies, resulting in a decrease in the surface tension and viscosity of the droplets and an increase in the saturation vapor pressure. The reduction in surface tension and viscosity reduces the surface binding force and internal viscous shear stress, promoting droplet spreading. Additionally, the increase in saturated vapor pressure enhances droplet evaporation and the vapor recoil-induced cutback, contributing to the decrease in the liquid–solid interface [37] and consequently reducing the dimensionless spreading diameter of the droplets. For the ethanol proportion at  $\omega_e = 0\%$  and  $\omega_e = 50\%$ , the maximum dimensionless spreading diameter of the droplets always increases with elevated surface temperature, and this phenomenon might be attributed to the effect of decreasing surface tension and viscosity, which has a dominant impact compared with the effect brought by the increasing saturated vapor pressure. However, when the ethanol proportion is at  $\omega_e = 100\%$ , with the increase in temperature, the saturated vapor pressure increases significantly, and after the substrate temperature increases from 393 K to 413 K, the decrease in the dimensionless spreading diameter due to the increase in the droplet's saturated vapor pressure takes the dominant position. Therefore, the dimensionless spreading diameter of the droplets decreases.

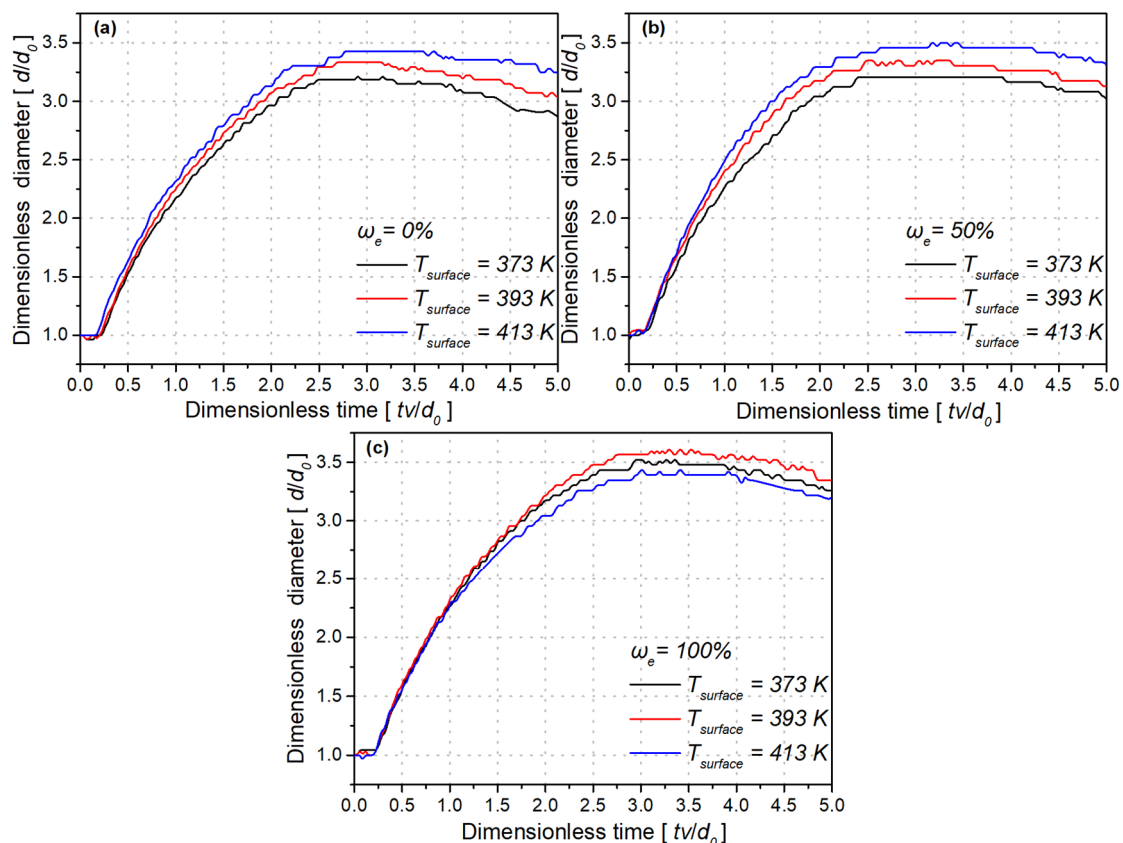


**Figure 7.** The effect of  $T_{surface}$  on the dimensionless spreading diameter of the droplet. (a)  $\omega_e = 0\%$ , (b)  $\omega_e = 50\%$ , (c)  $\omega_e = 100\%$ , (relative error less than  $\pm 5\%$ ).

Figure 8 illustrates the effect of ethanol proportion on the dimensionless spreading diameter of droplets with three different surface temperatures. As shown in Figure 8a,b, at a  $T_{surface}$  of 373 K and 393 K, the dimensionless spreading diameter of the droplet increases with the higher ethanol proportion. This is because the Weber number of the droplets increases with the higher ethanol concentration. Although the increase in the Reynolds

number and the saturated vapor pressure tends to reduce the dimensionless spreading diameter, their effect is weak due to the low superheat level. In Figure 8c, it can be seen that at a  $T_{surface}$  of 413 K, the dimensionless spreading diameter of the droplet first increases and then decreases, which is attributed to the high ethanol proportion. When the ethanol proportion increases from  $\omega_e = 50\%$  to  $\omega_e = 100\%$ , the reduction effect on the dimensionless spreading diameter due to vapor pressure increase reaches the peak, which overrules the promotion effect caused by the rise of the Weber number.

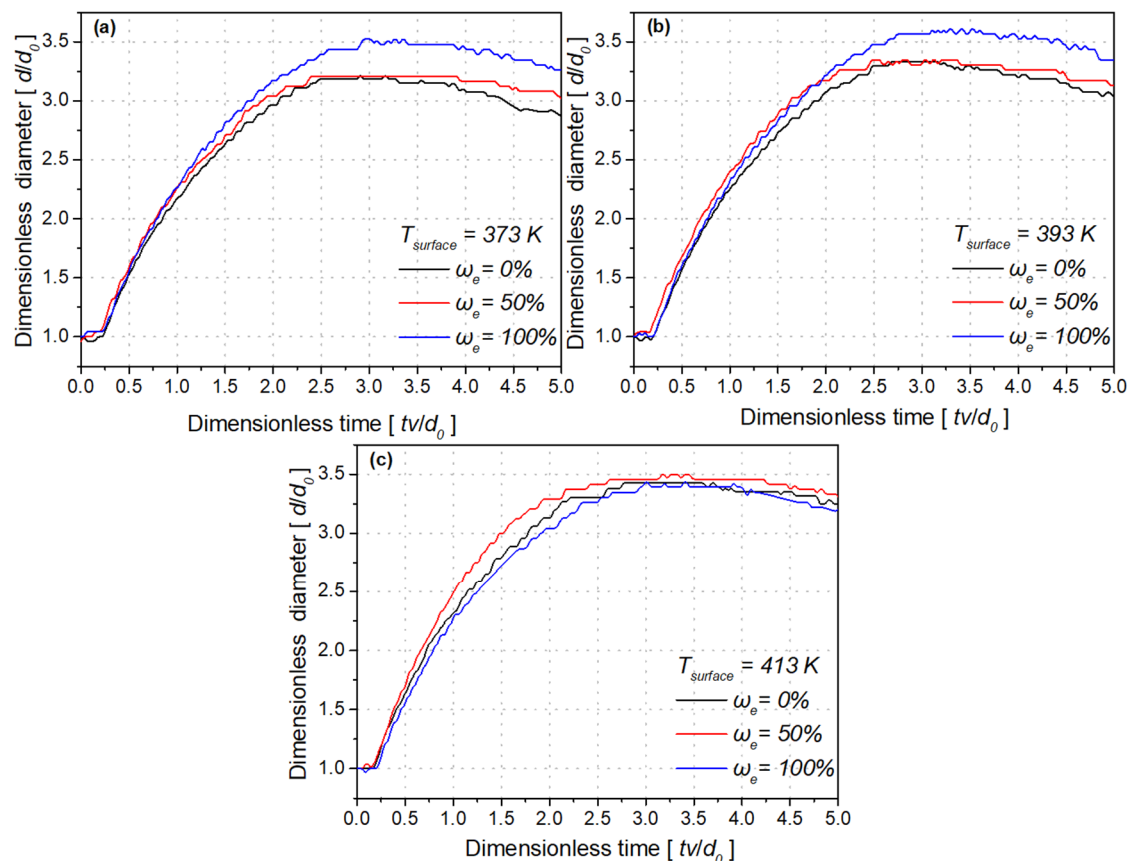


**Figure 8.** The effect of  $\omega_e$  on the dimensionless spreading diameter of the droplet. (a)  $T_{surface} = 373$  K, (b)  $T_{surface} = 393$  K, (c)  $T_{surface} = 413$  K, (relative error less than  $\pm 5\%$ ).

### 3.3. Droplet-Impinging Behaviors in Region B

In practical experimental conditions, it is impossible for the surface of the substrate glass slide to achieve absolute smoothness and cleanliness. Instead, the surface is likely to have some small cavities or impurities. These imperfections can increase the instability of the superheated liquid in the liquid–solid interface and create unstable sites in the interface. The nucleation energy barrier in these unstable sites is lower than in the rest of the liquid. As the superheat level increases, these unstable sites are the first to initiate the formation of boiling bubble nuclei, leading to partial boiling of the droplet, which is also known as puffing [38].

The photo sequence presented in Figure 9 depicts the droplet collision process in region B. During this process, the droplet undergoes collision and spreading behavior similar to region A. However, due to the formation of bubble embryos within the unstable site of the droplet, the droplets undergo partial boiling. Taking the images captured at 16.0 ms as an example, the emergence of “pagoda-like” bubble structures is observed, leading to the generation of puffing. Additionally, small jets are observed at the top of the “pagoda-like” vapor bubbles, which facilitate the ejection of daughter droplets. A similar “pagoda-like” bubble structure has also been mentioned in other studies [39,40], and this

kind of bubble structure was considered one of the main reasons for secondary atomization under this regime.

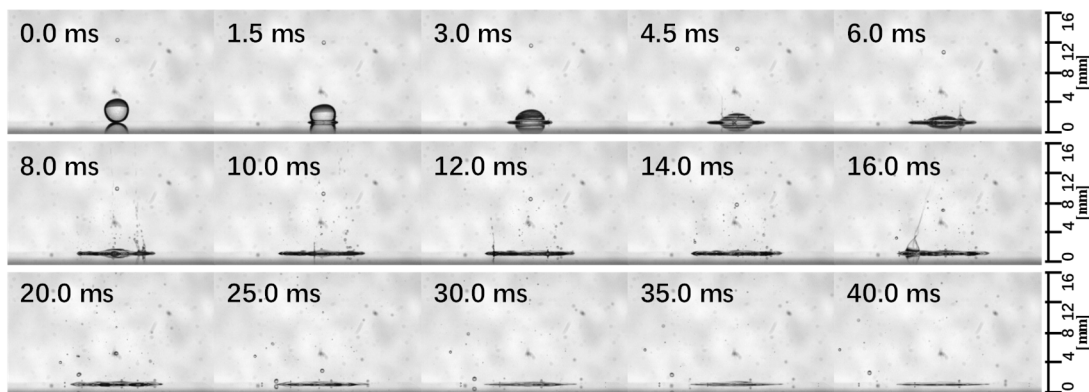


**Figure 9.** Photo sequence of the collision behavior in region B ( $\omega_e = 50\%$ ,  $T_{surface} = 493 \pm 5$  K).

As the location of the unstable site on the liquid–solid interface is related to the presence of imperfections, the locations of partial boiling vary. It is noteworthy that the photo sequence shows only one or two sites on the liquid–solid interface experiencing puffing at the same time, indicating that the substrate glass slide used in the experiment has good surface smoothness and cleanliness.

### 3.4. Droplet-Impinging Behaviors in Region C

As the superheat level increases further, the temperature of the liquid within the liquid–solid interface exceeds its superheat limit. This leads to a sharp increase in the number of critical bubble nuclei [41], leading to the generation of a large number of bubbles within the droplet and resulting in explosive flash boiling.

Figure 10 illustrates the droplet collision process in region C. During this process, the droplets undergo explosively flashing boiling, leading to the formation of coronal splashing. The reason for this coronal splashing is that the droplet spreads outward along the direction away from the impact point and breaks up due to boiling, causing the radial velocity from the droplet spreading and the upward velocity from the boiling breakup to combine and produce a coronal shape of the resulting droplets. Due to the generation of numerous bubble nuclei within the droplets on the liquid–solid interface, the space for each bubble is restricted, leading to the absence of the “pagoda-like” bubble structure observed in region B. In the photograph at 1.5 ms in Figure 10, it also can be seen that the droplet begins to boil immediately upon contact with the surface. This indicates that the heat transfer within the liquid–solid interface is extremely rapid, and the liquid at the contact surface is rapidly heated to above its superheat limit temperature.

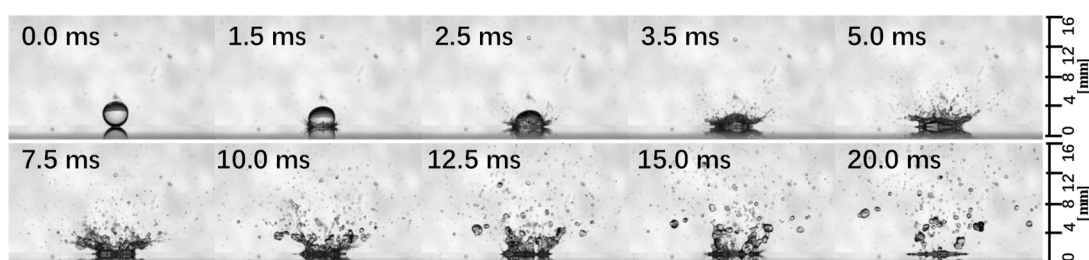


**Figure 10.** Photo sequence of the collision behavior in region C ( $\omega_e = 30\%$ ,  $T_{surface} = 533 \pm 5$  K).

In the photographs at region C in Figure 5, it can be observed that the droplets with an ethanol proportion of  $\omega_e = 30\%$  exhibit the most intense boiling. This behavior can be attributed to the deviation in the ethanol proportion of the liquid–vapor phase during



the phase change in the ethanol solution. This deviation leads to different amounts of superheat energy available for the vaporizable component in droplets with different ethanol proportions. In our previous flash boiling spray experiments, the most intense boiling behavior was also observed with an ethanol proportion of  $\omega_e = 30\%$ . A comprehensive analysis has been conducted to elucidate this phenomenon, and more details can be found in our previous publications [42].

### 3.5. Droplet-Impinging Behaviors in Region D

When the substrate surface temperature exceeds the droplet Leidenfrost temperature, a stable vapor film is formed in the liquid–solid interface. The droplet then floats on this vapor film, losing the wetting ability.

Figure 11 displays a photo sequence that illustrates the collision process of the droplet in region D. Upon impact, the droplet spreads outwardly, creating a cavity in the center of the disk-shaped droplet, as observed in the images taken at 10 ms. As the droplet spreading diameter reaches a maximum extent, it retracts from the periphery while rising vertically upward from the center, ultimately exhibiting a rebound. The mechanism of droplet collision behavior is such that as the droplet collides with the surface, the momentum of the radially spreading droplet exceeds its reactive force supplied by surface tension and viscosity, resulting in the droplet spreading on the surface. The reactive force provided by surface tension and viscosity gradually increases as the droplet spreads, while the impact force decreases. The droplet begins to retract and rebound from the surface when the surface tension and viscosity forces reach the maximum, and with the droplet retracting, the internal pressure of the droplet increases, which causes the droplet to relieve this pressure by rebounding upward from the surface. Owing to the vapor film's isolation, the droplet cannot directly contact the substrate surface, making it extremely difficult to form a bubble nucleus, which precludes boiling throughout the process. Additionally, the images captured at 2.0 ms and 4.0 ms show that the upper portion of the droplet also exhibits circular ripples produced by the compression of the liquid during the impact process. Furthermore, a comparison of the images in region A and D in Figure 5 indicates that the spreading extent of the droplet in region D is significantly reduced due to the loss of wetting between the liquid–solid interface caused by the vapor film's isolation.

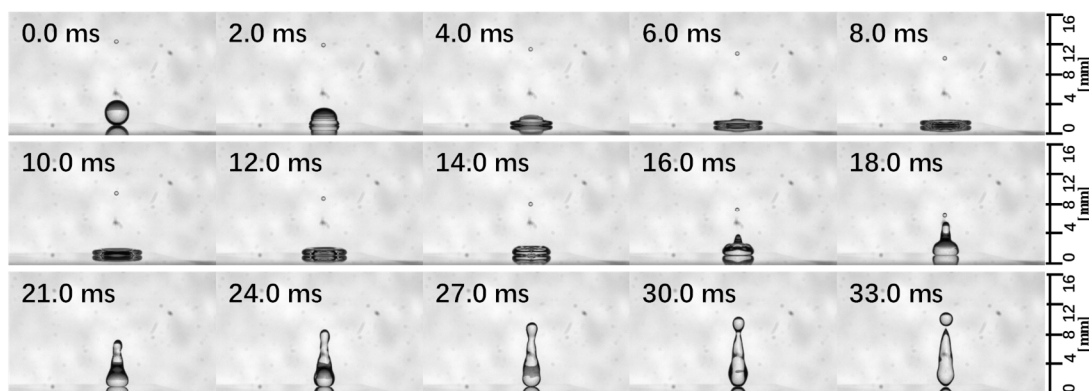


**Figure 11.** Photo sequence of the collision behavior in region D ( $\omega_e = 70\%$ ,  $T_{surface} = 533 \pm 5$  K).

Figure 12 illustrates the time evolutions of the dimensionless diameters and heights of droplets at various  $T_{surface}$  and  $\omega_e$  values. In Figure 12a, the droplet diameters increase with time, reach a maximum extent, and then decrease. In contrast, in Figure 12b, the droplet heights decrease with time, reach a minimum extent, and then increase. These curves depict that the droplets first spread and then rebound. When the ethanol proportion is held constant, the dimensionless diameter and height of the droplet do not show significant changes with surface temperature variations. This is due to the presence of the vapor film that impedes the heat transfer from the hot surface to the liquid, leading to an insignificant effect of the surface temperature on the liquid behavior. However, a significant difference



is observed between the results of the two ethanol proportions. The maximum spreading extent of the droplet increases with an increase in ethanol proportion, while the time required for the droplet to reach the maximum spreading extent decreases. Additionally, the height of the droplet during the rebound decreases with an increase in ethanol concentration. As the liquid is almost isolated from the hot surface by a vapor film, its dynamic behavior is only related to the Weber number. Since surface tension reduces the momentum of the radially spreading liquid and promotes retraction and rebound, the dimensionless diameter of the droplets is smaller, and the dimensionless height of the droplets is higher for a smaller Weber number.

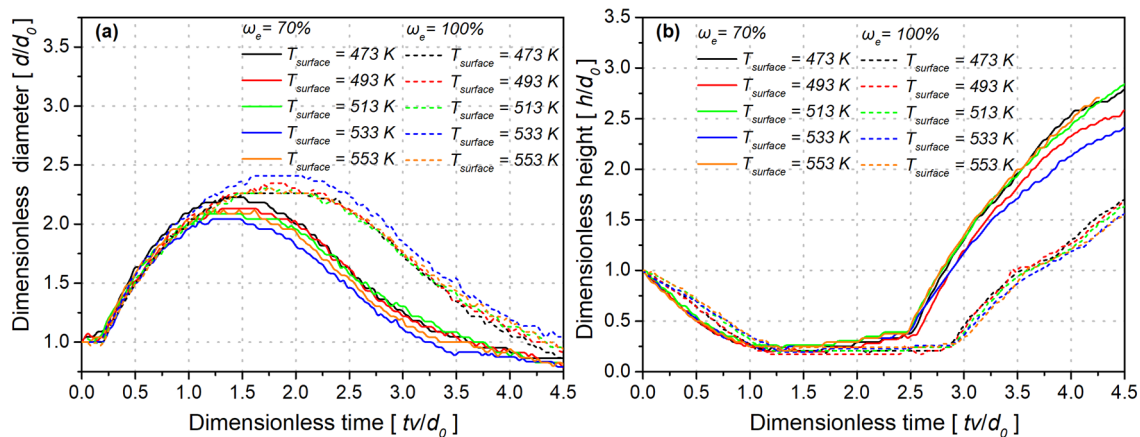


**Figure 12.** The time evolutions of the dimensionless spreading diameter and height at various  $T_{surface}$  and  $\omega_e$  values. (a) dimensionless diameter, (b) dimensionless height, (relative error less than  $\pm 5\%$ ).

### 3.6. Analysis of the Generality of Parameters in Describing Droplet Collision Behaviors

The superheat level  $R_p$  has been utilized in some previous studies to correlate the phase change regimes of liquids [33,43,44]. According to the results in the present study, when only one of the two conditions, ethanol proportion or substrate surface temperature, changes,  $R_p$  provides a good correlation with droplet collision behavior. As  $R_p$  increases, the droplet collision behavior shifts from region A to B, C, and D in the end. However, when both the ethanol proportion and the substrate surface temperature are varied,  $R_p$  lacks generality in describing droplet impact behaviors. For example, a droplet under the condition of  $\omega_e = 0\%$  and  $T_{surface} = 533$  K undergoes explosive flash boiling, while a droplet under the condition of  $\omega_e = 70\%$  and  $T_{surface} = 493$  K exhibits the Leidenfrost effect. Despite their different collision behaviors, both droplets have the same  $R_p$ . Therefore, the results in the present study indicate that the superheat level ( $R_p$ ) of a droplet at the substrate surface temperature lacks generality in describing the behaviors of a liquid droplet impinging on a hot surface.

In addition to  $R_p$ , the Weber number and the Reynolds number are also limited in their ability to describe droplet collision behavior, as their predictions may only be applicable within certain ranges of conditions. For instance, the Weber number shows good agreement with the maximum droplet spreading extent and rebound height in region D but does not correlate in region A. There is no correlation in regions A or D for the Reynolds number.

In summary, it is difficult to correlate the collision behavior of droplets to a single parameter for the overall droplet behavior. In fact, the collision behavior of the droplets is influenced by various factors, including heat transfer performance, volatility, viscosity, surface tension performance, and boiling characteristics. However, under certain conditions, it is feasible to predict droplet behavior by using only a single parameter. For example, the shift in different behavior regions can be linked solely to  $R_p$  under certain conditions, i.e., when only one of the two conditions, ethanol proportion or substrate surface temperature, changes, and this shift has no obvious relationship with the Reynolds number and the We-

ber number. Moreover, the spreading or rebounding behavior of the droplets can be linked solely to the Weber number under certain conditions, i.e., in the Leidenfrost effect region.

#### 4. Conclusions

In this paper, the dynamic behaviors of a hydrous ethanol droplet impinging on a heated horizontal glass surface were experimentally investigated under a wide range of conditions. Based on the results, the following conclusions were obtained:

- (1) The addition of volatile ethanol to less volatile water can promote a shift in droplet collision behaviors from quiescent surface evaporation (with spreading) to explosive boiling, and eventually to the Leidenfrost phenomenon. As the ethanol mass fraction ( $\omega_e$ ) increased from 0% to 100%, the superheat limit temperature decreased by approximately 80 K, while the Leidenfrost temperature decreased by at least 100 K.
- (2) Four regions were clearly identified for surface temperature ( $T_{surface}$ ) ranging from 373 K to 553 K, and the ethanol mass fraction ( $\omega_e$ ) varied from 0% to 100%. In region A, the droplets just spread with quiescent surface evaporation. In region B, the puffing or partial boiling occurred as the droplets spread. In region C, the droplets reacted by explosive nuclear boiling. In region D, the wettability disappeared, and the droplet rebounded due to the Leidenfrost effect.
- (3) The dimensionless diameter of a droplet in region A is determined by the combined effect of surface temperature, surface tension, and viscosity. In region D, the dimensionless diameter and height of the droplet are mainly influenced by its surface tension. The droplets of lower ethanol concentrations rebounded faster and higher due to their lower surface tensions.
- (4) Although  $R_p$ , the Weber number, and the Reynolds number lack the generality to describe overall droplet collision behaviors, it is feasible to predict partial collision behaviors by using one of them under certain conditions. For drops with low-impact Weber numbers (Weber number < 40), when only one of the two conditions, ethanol proportion or substrate surface temperature, changes,  $R_p$  provides a good correlation with the shift in different behavior regions. For drops in the Leidenfrost effect region, the Weber number provides a good correlation with the spreading or rebounding behavior of the droplets.

**Author Contributions:** Conceptualization, Z.Z.; investigation, Z.Z.; methodology, Z.Z. and D.W.; software, G.Z.; data curation, G.Z. and Z.Z.; visualization, Z.Z. and G.Z.; writing—original draft preparation, Z.Z.; writing—review and editing, D.W., H.X. and F.Y.; supervision, D.W. and F.Y.; funding acquisition, F.Y., H.X. and D.W. All authors have read and agreed to the published version of the manuscript.

**Funding:** This work is supported by “UK EPSRC project (EP/S00193X/2)” and “China Scholarships Council (No. 202006950035)”.

**Data Availability Statement:** Not applicable.

**Acknowledgments:** The authors would like to express their thanks to the Future Engine and Fuels Lab at the University of Birmingham for the materials and equipment they provided for this study. The authors also would like to express gratitude to the Advanced Manufacturing Technology Centre at the University of Birmingham for the technical help from Themistoklis Karkantonis.

**Conflicts of Interest:** The authors declare no conflict of interest.

#### References

1. Mudawar, I. Assessment of high-heat-flux thermal management schemes. *IEEE Trans. Compon. Packag. Technol.* **2001**, *24*, 122–141. [[CrossRef](#)]
2. Pasandideh-Fard, M.; Aziz, S.D.; Chandra, S.; Mostaghimi, J. Cooling effectiveness of a water drop impinging on a hot surface. *Int. J. Heat Fluid Flow* **2001**, *22*, 201–210. [[CrossRef](#)]
3. Moreira, A.L.N.; Moita, A.S.; Panão, M.R. Advances and challenges in explaining fuel spray impingement: How much of single droplet impact research is useful? *Prog. Energy Combust. Sci.* **2010**, *36*, 554–580. [[CrossRef](#)]

4. Zhang, G.; Shi, P.; Luo, H.; Ogata, Y.; Nishida, K. Investigation on fuel adhesion characteristics of wall-impingement spray under cross-flow conditions. *Fuel* **2022**, *320*, 123925. [\[CrossRef\]](#)
5. Zhang, G.; Si, Z.; Zhai, C.; Luo, H.; Ogata, Y.; Nishida, K. Characteristics of wall-jet vortex development during fuel spray impinging on flat-wall under cross-flow conditions. *Fuel* **2022**, *317*, 123507. [\[CrossRef\]](#)
6. Liu, H.; Cai, C.; Jia, M.; Gao, J.; Yin, H.; Chen, H. Experimental investigation on spray cooling with low-alcohol additives. *Appl. Therm. Eng.* **2019**, *146*, 921–930. [\[CrossRef\]](#)
7. Luo, H.; Jin, Y.; Nishida, K.; Ogata, Y.; Yao, J.; Chen, R. Microscopic characteristics of impinging spray sliced by a cone structure under increased injection pressures. *Fuel* **2021**, *284*, 284. [\[CrossRef\]](#)
8. Luo, H.; Chang, F.; Zhan, C.; Nishida, K.; Ogata, Y.; Zhang, J.; Yao, J.; Kong, X.; Zhu, J. Microscopic characteristics of multiple droplets behaviors at the near-wall region during the quasi-steady state. *Fuel* **2021**, *286*, 119431. [\[CrossRef\]](#)
9. Mundo, C.; Sommerfeld, M.; Tropea, C. Droplet-wall collisions: Experimental studies of the deformation and breakup process. *Int. J. Multiph. Flow* **1995**, *21*, 151–173. [\[CrossRef\]](#)
10. An, S.M.; Lee, S.Y. Maximum spreading of a shear-thinning liquid drop impacting on dry solid surfaces. *Exp. Therm. Fluid Sci.* **2012**, *38*, 140–148. [\[CrossRef\]](#)
11. Andrade, R.; Skurtys, O.; Osorio, F. Experimental study of drop impacts and spreading on epicarps: Effect of fluid properties. *J. Food Eng.* **2012**, *109*, 430–437. [\[CrossRef\]](#)
12. Abubakar, A.A.; Yilbas, B.S.; Al-Qahtani, H.; Mohammed, A.S. Liquid Droplet Impact Over Hydrophobic Mesh Surfaces and Assessment of Weber Number Dependent Characteristics. *J. Fluids Eng.* **2022**, *144–155*, 144–155. [\[CrossRef\]](#)
13. Abubakar, A.A.; Yilbas, B.S.; Qahtani, M.H.A.; Hassan, G.; Yakubu, M.; Bahatab, S.; Adukwu, J.A.E. Experimental and Model Studies of Various Size Water Droplet Impacting on a Hydrophobic Surface. *J. Fluid Eng.-T. Asme.* **2021**, *163*, 061402. [\[CrossRef\]](#)
14. Josserand, C.; Lemoyne, L.; Troeger, R.; Zaleski, S. Droplet impact on a dry surface: Triggering the splash with a small obstacle. *J. Fluid Mech.* **2005**, *524*, 47–56. [\[CrossRef\]](#)
15. Yarin, A.L. Droplet impact dynamics: Splashing, Spreading, Receding, Bouncing. *Annu. Rev. Fluid Mech.* **2006**, *38*, 159–192. [\[CrossRef\]](#)
16. Bernardin, J.D.; Stebbins, C.J.; Mudawar, I. Mapping of impact and heat transfer regimes of water drops impinging on a polished surface. *Int. J. Heat Mass Transf.* **1997**, *40*, 247–267. [\[CrossRef\]](#)
17. Choi, K.J.; Yao, S.C. Mechanisms of film boiling heat transfer of normally impacting spray. *Int. J. Heat Mass Transf.* **1987**, *30*, 311–318. [\[CrossRef\]](#)
18. Avedisian, C.T. On the collision of a droplet with a solid surface. *Proc. R. Soc. Lond. Ser. A Math. Phys. Sci.* **1997**, *432*, 13–41. [\[CrossRef\]](#)
19. Grissom, W.M.; Wierum, F.A. Liquid spray cooling of a heated surface. *Int. J. Heat Mass Transf.* **1981**, *24*, 261–271. [\[CrossRef\]](#)
20. Qiao, Y.M.; Chandra, S. Experiments on adding a surfactant to water drops boiling on a hot surface. Proceedings of the Royal Society of London Series A: Mathematical. *Phys. Eng. Sci.* **1997**, *453*, 673–689. [\[CrossRef\]](#)
21. Chandra, S.; di Marzo, M.; Qiao, Y.M.; Tartarini, P. Effect of liquid-solid contact angle on droplet evaporation. *Fire Saf. J.* **1996**, *27*, 141–158. [\[CrossRef\]](#)
22. Fujimoto, H.; Oku, Y.; Ogihara, T.; Takuda, H. Hydrodynamics and boiling phenomena of water droplets impinging on hot solid. *Int. J. Multiph. Flow* **2010**, *36*, 620–642. [\[CrossRef\]](#)
23. Li, J.; Weisensee, P. Droplet impact and Leidenfrost dynamics on a heated post. *Int. J. Heat Mass Transf.* **2023**, 201–212. [\[CrossRef\]](#)
24. Roisman, I.V.; Breitenbach, J.; Tropea, C. Thermal atomisation of a liquid drop after impact onto a hot substrate. *J. Fluid Mech.* **2018**, *842*, 87–101. [\[CrossRef\]](#)
25. Zhang, W.-W.; Li, Y.-Y.; Long, W.-J.; Cheng, W.-L. Enhancement mechanism of high alcohol surfactant on spray cooling: Experimental study. *Int. J. Heat Mass Transf.* **2018**, *126*, 363–376. [\[CrossRef\]](#)
26. Shi, X.; Qian, W.; Liao, Y.; Ma, X.; Wang, Q.; Ni, J. Experimental and Simulation Analysis on Spray Characteristics of Hydrous Ethanol–Gasoline Blends. *J. Energy Resour. Technol.* **2022**, *144*, 112302. [\[CrossRef\]](#)
27. Liu, L.; Liu, Y.; Mi, M.; Wang, Z.; Jiang, L. Evaporation of a bicomponent droplet during depressurization. *Int. J. Heat Mass Transf.* **2016**, *100*, 615–626. [\[CrossRef\]](#)
28. Blanken, N.; Saleem, M.S.; Thoraval, M.-J.; Antonini, C. Impact of compound drops: A perspective. *Curr. Opin. Colloid Interface Sci.* **2021**, *51*, 101389. [\[CrossRef\]](#)
29. Piskunov, M.; Semyonova, A.; Khomutov, N.; Ashikhmin, A.; Yanovsky, V. Effect of rheology and interfacial tension on spreading of emulsion drops impacting a solid surface. *Phys. Fluids* **2021**, *33*, 83309. [\[CrossRef\]](#)
30. Renon, H.; Prausnitz, J.M. Local compositions in thermodynamic excess functions for liquid mixtures. *AIChE J.* **1968**, *14*, 135–144. [\[CrossRef\]](#)
31. ASPEN Technology. *Aspen Plus®: Aspen Plus User Guide*, Version 11.1; Aspen Technology, Inc.: Bedford, MA, USA, 2001.
32. Seki, M.; Kawamura, H.; Sanokawa, K. Transient Temperature Profile of a Hot Wall Due to an Impinging Liquid Droplet. *J. Heat Transf.* **1978**, *100*, 167–169. [\[CrossRef\]](#)
33. Wang, B.; Wang, Z.; Bao, X.; Li, Y.; Jiang, Y.; Xu, H.; Zhang, X. Microscopic investigation of near-field spray characteristics of 2-methylfuran, ethanol and isooctane under flash boiling conditions. *Fuel* **2018**, *215*, 142–152. [\[CrossRef\]](#)
34. Rein, M. Phenomena of liquid drop impact on solid and liquid surfaces. *Fluid Dyn. Res.* **1993**, *12*, 61–93. [\[CrossRef\]](#)

35. Wachters, L.H.J.; Westerling, N.A.J. The heat transfer from a hot wall to impinging water drops in the spheroidal state. *Chem. Eng. Sci.* **1966**, *21*, 1047–1056. [[CrossRef](#)]
36. Otsu, N. A Threshold Selection Method from Gray-Level Histograms. *IEEE Trans. Syst. Man Cybern.* **1979**, *9*, 62–66. [[CrossRef](#)]
37. Kandlikar, S.G.; Steinke, M.E. Contact angles and interface behavior during rapid evaporation of liquid on a heated surface. *Int. J. Heat Mass Transf.* **2002**, *45*, 3771–3780. [[CrossRef](#)]
38. Zhang, X.; Li, T.; Wang, B.; Wei, Y. Superheat limit and micro-explosion in droplets of hydrous ethanol-diesel emulsions at atmospheric pressure and diesel-like conditions. *Energy* **2018**, *154*, 535–543. [[CrossRef](#)]
39. Cossali, G.E.; Marengo, M.; Santini, M. Secondary atomisation produced by single drop vertical impacts onto heated surfaces. *Exp. Therm. Fluid Sci.* **2005**, *29*, 937–946. [[CrossRef](#)]
40. Moita, A.S.; Moreira, A.L.N. The combined effects of surface topography and heat transfer on the droplet/wall interaction mechanisms. In Proceedings of the 20th Annual Conference on Liquid Atomisation and Spray Systems-ILASS, Vail, CO, USA, 26–30 July 2005; pp. 431–436.
41. Avedisian, C.T. The Homogeneous Nucleation Limits of Liquids. *J. Phys. Chem. Ref. Data* **1985**, *14*, 695–729. [[CrossRef](#)]
42. Zhou, Z.; Li, Y.; Zhang, J.; Wang, Y.; Yan, F.; Xu, H. Effects of component proportions on multi-jet instant expansion of binary solutions under flash boiling conditions. *Fuel* **2021**, *308*, 122018. [[CrossRef](#)]
43. Araneo, L.; Donde, R. Flash boiling in a multihole G-DI injector—Effects of the fuel distillation curve. *Fuel* **2017**, *191*, 500–510. [[CrossRef](#)]
44. Aori, G.; Hung, D.L.S.; Zhang, M.; Zhang, G.; Li, T. Effect of Nozzle Configuration on Macroscopic Spray Characteristics of Multi-Hole Fuel Injectors under Superheated Conditions. *At. Spray* **2016**, *26*, 439–462. [[CrossRef](#)]

**Disclaimer/Publisher’s Note:** The statements, opinions and data contained in all publications are solely those of the individual author(s) and contributor(s) and not of MDPI and/or the editor(s). MDPI and/or the editor(s) disclaim responsibility for any injury to people or property resulting from any ideas, methods, instructions or products referred to in the content.